CFD–RANS analysis of the rotational effects on the boundary layer of wind turbine blades

Journal of Physics: Conference Series **75** (2007) 012031 doi:10.1088/1742-6596/75/1/012031

CFD–RANS analysis of the rotational effects on the boundary layer of wind turbine blades

Carlo E Carcangiu[1, 2], Jens N Sørensen[1], Francesco Cambuli[2] and Natalino Mandas[2]

[1] Dept. of Mechanical Engineering, DTU, Bld. 403, Lyngby–2800, Denmark
[2] Dept. of Mechanical Engineering, Univ. of Cagliari, Piazza d'Armi 1, Cagliari–09121, Italy

E-mail: carcangiu@dimeca.unica.it

Abstract. The flow field past the rotating blade of a horizontal axis wind turbine has been modeled with a full 3–D steady–RANS approach. Flow computations have been performed using the commercial finite–volume solver Fluent. A number of blade sections from the 3–D rotating geometry were chosen and the corresponding 2–D flow computations have been carried out for comparison, for different angles of attack and in stalled conditions. In order to investigate the effects of rotation a postprocessing tool has been developed, allowing the evaluation of the terms in the boundary layer equations. Examples of the output are proposed for the analyzed flow situations. The main features of the boundary layer flow are described, for both the rotating blade and the corresponding 2–D profiles. Computed pressure distributions and aerodynamic coefficients evidence less lift losses after separation in the 3–D rotating case, mostly for the inward sections of the blade and the highest angles of attack, in agreement with the literature.

1. Introduction

Wind turbine blades are strongly affected by rotational and 3–D flow effects and they often operate in deep stall. Nevertheless, the actual design approach is typically based on employing the blade–element momentum–theory (BEM), with lift and drag forces determined from 2–D measurements. The results obtained are reasonable accurate in the proximity of the design point, but in stalled condition the BEM is known to underpredict the forces acting on the blades, as shown in the literature (see, *e.g.* [1]). Furthermore, the accurate prediction of rotor loads even in stalled conditions is of great importance for sizing the generator and other mechanical components.

The radial flow component present in the bottom of separated boundary layers of rotating wings is the reason of altered lift and drag characteristics of the individual blade sections with respect to the 2–D airfoils [2]. Two main contributions are commonly indicated for the rise of those phenomena, but the discussion about them is still open. One is Coriolis force, which acts in the chordwise direction as a favorable pressure gradient that tends to delay separation. On the other hand, centrifugal forces produce a spanwise pumping effect, resulting mainly in boundary layer thinning.

The present work aims at giving a better understanding of the main influence of rotational effects on the boundary layer that develops over wind turbine blades.

In 1945 Himmelskamp [3] first described through measurements the 3–D and rotational effects on the boundary layer a rotating propeller, finding lift coefficients much higher moving toward

the rotational axis. Further experimental studies confirmed these early results, indicating in stall–delay and post–stalled higher lift coefficient values the main effects of rotation on wings. Measurements on wind turbine blades were performed by Ronsten [4], showing the differences between rotating and non–rotating pressure coefficients and aerodynamic loads and by Tangler and Kocurek [5], who combined results from measurements with the classical BEM method to properly compute lift and drag coefficients and the rotor power in stalled conditions.
The theoretical foundations for the analysis of the rotational effects on rotating blades come to the late 40's, with Sears [6], who derived a set of equation for the potential flow field around a cylindrical blade of infinite span in pure rotation. He stated that the spanwise component of velocity is dependent only upon the potential flow and it is independent of the span (the so–called *independence principle*). Then, Fogarty and Sears [7] extended the former study to the potential flow around a rotating and advancing blade. They confirmed that, for a cylindrical blade advancing like a propeller, the tangential and axial velocity components are the same as in the 2–D motion at the local relative speed and incidence. A more comprehensive work was made once more by Fogarty [8], consisting of numerical computations on the laminar boundary layer of a rotating plate and blade with thickness. Here he showed that the separation line is unaffected by rotation and that the spanwise velocities in the boundary layer appeared small compared to the chordwise, and no large effects of rotation were observed, in contrast to [3]. A theoretical analysis was done by Banks and Gadd [9], focussed on demonstrating how rotation delays laminar separation. They found that the separation point is postponed due to rotation, and for extreme inboard stations the boundary layer is completely stabilized against separation. In the NASA report done by McCroskey and Dwyer [10], the so-called secondary effects in the laminar incompressible boundary layer of propeller and helicopter rotor blades are widely studied, by means of a combined numerical and analytical approach. They showed that approaching the rotational axis, the Coriolis force in the crossflow direction becomes more important. On the other hand the centrifugal pumping effect is much weaker than generally was supposed before, but its contribution increases as the magnitude of the adverse pressure gradient increases.
The last two decades have known the rising of computational fluid dynamic and the study of the boundary layer on rotating blade has often been carried on through a numerical approach. Twenty years ago, Sørensen [11] numerically solved the 3–D equations of the boundary layer on a rotating surface, using a viscous–inviscid interaction model. In his results the position of the separation line still appears the same as for 2–D predictions, but where separations are more pronounced a larger difference between the lift coefficient calculated for the 2–D and 3–D case is noticed. A quasi 3–D approach, based on the viscous–inviscid interaction method, was introduced by Snel *et al.* [1] and results were compared with measurements. They proposed a semi–empirical law for the correction of the 2–D lift curve, identifying the local chord to radii (c/r) ratio of the blade section as the main parameter of influence. This result has been confirmed by Shen and Sørensen [12] and by Chaviaropoulos and Hansen [13], who performed airfoil computations applying a quasi 3–D Navier–Stokes model, based on the streamfunction–vorticity formulation. Du and Selig [14] approached the problem solving the 3–D incompressible steady boundary layer equations. Their analysis stated that the stall delay depends slightly on the pressure effect and mainly on the acceleration of the boundary layer flow, *i.e.* on the Coriolis forces. Both rotational effects become smaller going outward according with [12] and [13]. Hu and co–workers [15] carried on a study of the stall–delay for wind turbines by means of boundary layer analysis, full N–S computations and wind tunnel experiments. The boundary layer analysis results in an extension of the work by Snel *et al.* [1]; for the full N–S computation the commercial code Fluent has been used, modeling the geometry accordingly to the experimental set–up.
3–D correction of 2–D airfoil characteristics has been made by Lindenburg [16], taking the local speed ratio into account and introducing a drag force correction, and by Bak *et al.* [17], using the different pressure distributions of rotating and non-rotating airfoils. Both of these papers

present a comparison with experimental data.
The paper is organized as follows. The governing equations, the numerical model and the postprocessing tool are presented in Section 2. All the results are shown and discussed in Section 3.

2. Methods

Making use of a commercial CFD code, the governing equations for the viscous incompressible 3–D flow field around a rotating blade of a wind turbine have been solved, considering a non–inertial reference system moving with the rotor. 3–D and 2–D turbulent flow simulations were performed, with different angles of attack. The rotational speed is constant for all the computations, $\Omega = 3$ rad/s. A non–twisted and zero–pitched blade was used and a non–uniform incoming flow was considered (Figure 1). The geometric angle of attack is kept constant along the span by specifying the axial flow component as $(\Omega z)/V(z) = const$, where z is the radial coordinate and Ω the rotational speed. The idea is to built a database of different flow conditions, varying angle of attack, Reynolds number and radial position. In order to analyze the output data, an ad–hoc postprocessing tool has been developed, allowing the evaluation within the computational domain of all the terms in a modified form of the Prandtl's boundary layer equation.

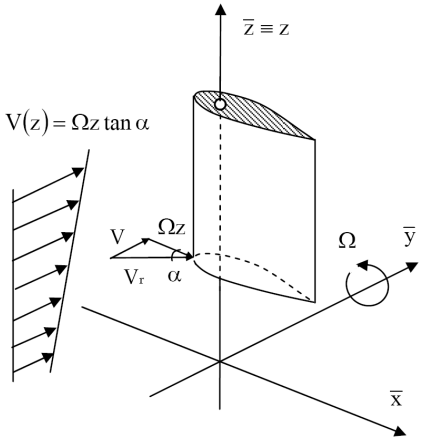

Figure 1. Incoming wind velocity profile.

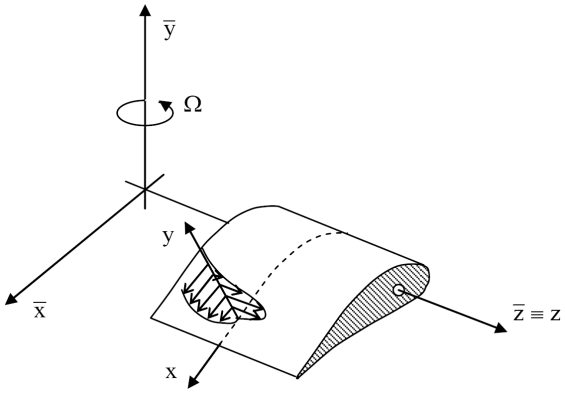

Figure 2. Reference systems of coordinates, global $(\bar{x}, \bar{y}, \bar{z})$ and local (x, y, z).

2.1. Mathematical model

Consider a blade section performing a steadily rotating motion. Two different reference systems are now introduced. One is a global reference system attached with the blade and moving with that. The second one is a local reference system, still fixed with the blade, but aligned point by point with the local tangential and normal directions of the blade surface (Figure 2). In the first system the steady incompressible time–averaged Navier–Stokes equations (see *e.g.* [19]) for a rotating frame of reference are defined and numerically solved

$$\nabla \cdot \vec{V_r} = 0 \tag{1}$$

$$\nabla \cdot (\vec{V_r}\vec{V_r}) + 2\vec{\Omega} \times \vec{V_r} + \vec{\Omega} \times \vec{\Omega} \times \vec{r} = -\frac{1}{\rho}\nabla p + \nabla \cdot \tau + \vec{f} \tag{2}$$

where we have: the relative velocity vector $\vec{V_r}$, the rotational speed $\vec{\Omega}$, the fluid density ρ, the stress tensor τ and the external body–forces $\vec{f}$. Let us identify then the Coriolis force term $2\vec{\Omega} \times \vec{V_r}$ and the centrifugal force term $\vec{\Omega} \times \vec{\Omega} \times \vec{r}$.

The second reference system refers to the boundary layer equations, which will be recalled in the post–processing step.

2.2. Numerical model

All the computations have been performed using the finite–volume code Fluent 6.3 with a steady–RANS approach. One untwisted blade, consisting of a symmetric NACA 0018 airfoil with constant chord, has been modeled, by applying periodicity for the three–bladed rotor. The blade geometry has been scaled using a constant chord length, $C = 1\ m$. The radius is 2 C and 20 C, at the root and at the tip of the blade respectively. A computational domain enclosed by two cylinders has been chosen, with the blade starting at the inner cylinder and ending at the outer cylinder (Figure 3). The full axial extension of the domain is 2 times the rotor diameter and is centered on the blade. These proportions resulted from the best balance found between computational efforts and boundaries independency.

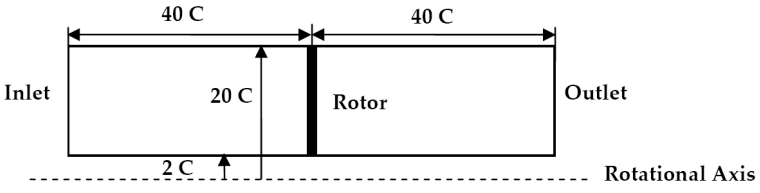

Figure 3. Computational domain (C = chord length).

The grid has been generated modularly with Gambit. It consists of a C–shaped region around the blade blended with a cylindrical external block. In the core, one counts 35 cells from the airfoil to a normal distance of approximately half–chord (with a first cell height of 10^{-5} chord length), 120 cells for each side of the profile and 45 cells along the spanwise direction. The boundary layer has been solved directly, with y^+ values limited between 1 and 3 and the κ–ω SST turbulence model by Menter has been used for turbulent computations. Dirichlet for velocity at the inlet and Neumann for pressure at the outlet were imposed as consistent boundary conditions, while the inner and outer cylindrical surfaces have been regarded as Euler–slip walls. In the 3–D case the standard grid had about one million control volumes and a refinement study was made with a two millions cells grid. With the same set–up 2D computations have been performed, in order to show differences and analogies. A fundamental problem is the determination of the actual angle of attack and the followed procedure is presented in the next paragraph.

2.3. Determination of 3–D angle of attack

The rotational effects could be studied and identified by comparing the full 3–D rotating blade computations with the corresponding 2–D situations. Nevertheless, the flow conditions in the two cases must be carefully chosen, i.e. in a consistent manner. It is well known that the flow similarity property could be achieved if the Reynolds number is kept the same, but in the theory of wing sections another key–parameter has to be considered, *i.e.* the angle of attack. Angle of attack is a 2–D concept. It is defined as the geometrical angle between the relative flow direction and the chord of the airfoil. Consequently, finding an equivalent local angle of attack for 3–D flows is not trivial. For a rotating blade, for instance, the flow passing by a blade section is influenced by the bound circulation on the blade. Moreover, a further complication arises from the 3–D effects from tip and root vortices, neglected for the sake of simplicity in our model. Here, to determine the local angle of attack from the computed 3–D flow field two different techniques were considered. The first technique is the averaging technique suggested in [20] and then, slightly modified, employed in [21]. The second technique has been recently proposed

by Shen *et al.* [22] as a method suitable for more general flow conditions and it is based on the determination of the local induced velocities created by bound vortices. After verifying the agreement between the outputs from the two strategies, the latter has been finally chosen for all further investigations.

2.4. Postprocessing tool

In order to analyze the output data from the N–S code a Matlab program has been developed, to evaluate the relative importance of the various terms in the boundary layer equations with respect to the arising of rotational effects. The 3–D incompressible boundary layer equations for a steady rotating flow, based on the Prandtl's boundary layer equations (see [18]), read

$$\frac{\partial u}{\partial x} + \frac{\partial v}{\partial y} + \frac{\partial w}{\partial z} = 0 \tag{3}$$

$$u\frac{\partial u}{\partial x} + v\frac{\partial u}{\partial y} + w\frac{\partial u}{\partial z} = -\frac{1}{\rho}\frac{\partial p}{\partial x} + 2\Omega w\cos\theta + \Omega^2\overline{x}\cos\theta + \frac{\partial}{\partial y}\left(\nu\frac{\partial u}{\partial y} - \overline{u'v'}\right) \tag{4}$$

$$u\frac{\partial w}{\partial x} + v\frac{\partial w}{\partial y} + w\frac{\partial w}{\partial z} = -\frac{1}{\rho}\frac{\partial p}{\partial z} + 2\Omega u\cos\theta + \Omega^2\overline{z} + \frac{\partial}{\partial y}\left(\nu\frac{\partial w}{\partial y} - \overline{v'w'}\right) \tag{5}$$

where (u, v, w) are the velocity components in directions (x, y, z), *i.e.* the axes of the local system of coordinates, and with theta defining the angle between the tangent to the airfoil and the $x - z$ plane. The desired output variables are computed in some proper surfaces of constant radius, extended to a distance of half chord length from the blade wall. The variables of interest are sorted in a new order, according to the boundary layer tangential and normal directions (see local system of coordinates in Figure 2). The derivatives are estimated taking a 2^{nd} order CDS polynomial fitting of the output data for non–uniform spaced grids. The boundary layer height is also found, checking both the vorticity magnitude and the velocity gradient values along the normal direction as diagnostic method. The last technique has been suggested by Stock and Haase [23].

3. Results and Discussion

The present section reports the analysis of the computed flow solution, focussed on the general features of the flow field around rotating blades and aimed at showing the effects of rotation, on pressure coefficient distributions and integral aerodynamic coefficients. Further studies are required for stating more about the specific goal of our project, however a first glance into the postprocessing phase is given. A number of different flow condition have been simulated and analyzed, with geometric angles of attack ranging from 0 to 16 degrees. The effective values of local angle of attack for inboard sections can be higher than 20 degrees and a large portion of the blade suction side is dominated by separation phenomena (Figure 4).

In the turbulent flow computations Reynolds number along the blade varies between $1 \cdot 10^6$ and $6 \cdot 10^6$ from root to tip. The radial stations chosen for the analysis are located at r/R = 0.16, 0.54 and 0.75. A detailed depiction of the boundary layer velocity profiles in a local coordinate system is available for different spanwise position along the blade. The pure rotating blade, without inflow and with zero pitch angle, is presented as a reference case in laminar flow regime. The velocity profiles shape (Figure 5) looks physically correct and the crossflow becomes important after separation, which in this case occurs near 80% of the chord length.

In Figure 6 the in–plane streamlines around the rotating blade section and the corresponding pure 2–D airfoil are plotted, in a situation of deep stall. It is visible that the main effects of rotation are to stabilize vortex shedding and limit the growth of the separation cell. Moreover, the stagnation point moves downstream, and separation tends to approach the leading edge. This

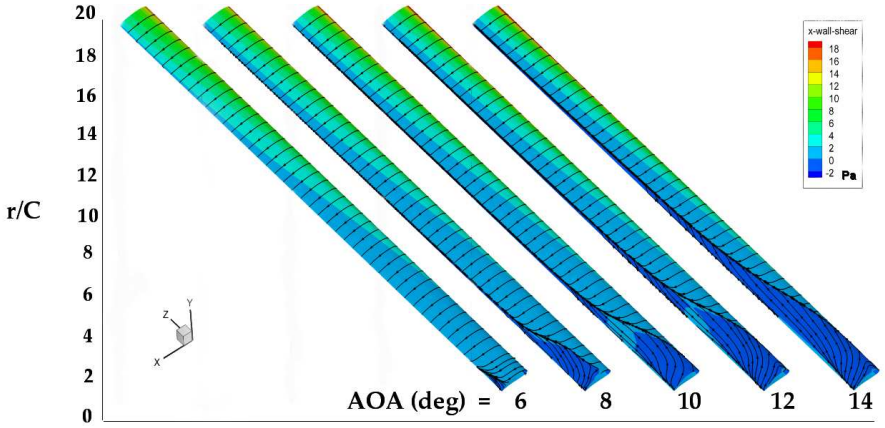

Figure 4. Limiting streamlines on blade suction side for different geometric flow incidences.

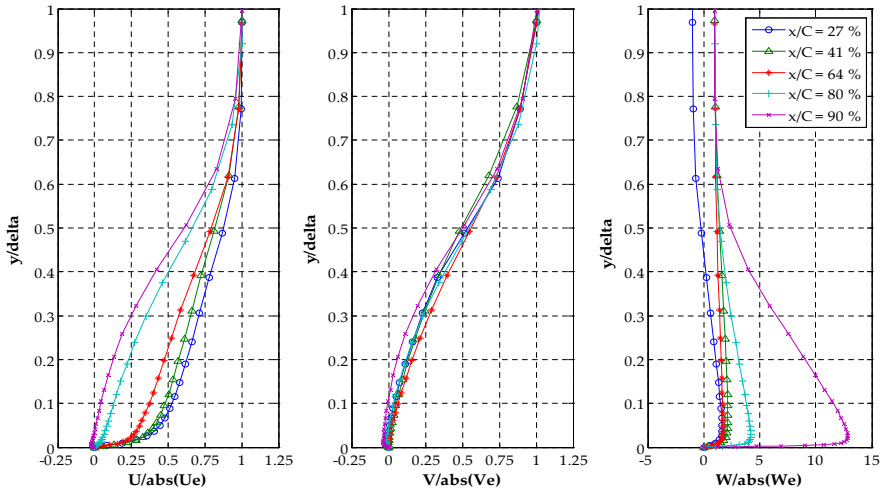

Figure 5. Velocity profiles in the local coordinate system, for different chordwise positions x/C, plotted against the non-dimensional boundary layer thickness y/δ and non-dimensionalised with the values at boundary layer edge (3–D, $r/R = 0.16$, AOA $= 13.4$ deg, $Re = 10^2$).

is confirmed by Figure 7, where pressure coefficients evaluated with 3–D and 2–D simulations have been compared.

As an example of the postprocessing output, the magnitude of the Coriolis and spanwise–convection terms in the governing equations have been evaluated (Figure 8). When separation occurs the rising of both these terms is found and generally Coriolis terms show higher values. A more comprehensive analysis on the boundary layer integral properties is still in progress, that could help in finding the most important causes of the rotational effects.

An important result of the postprocessing is the evaluation of aerodynamic coefficients (Figure 9). It is visible that lift losses are strongly reduced in post-stalled conditions by rotation, as much as higher the flow incidence is. On the other hand we registered higher values of drag coefficients. The results have been compared with a pure 2–D airfoil, showing that 3–D values are higher for the whole range of flow angles. However, the real 3–D rotating results differ from the reference for the lower angles of attack and attached flow conditions. This might be

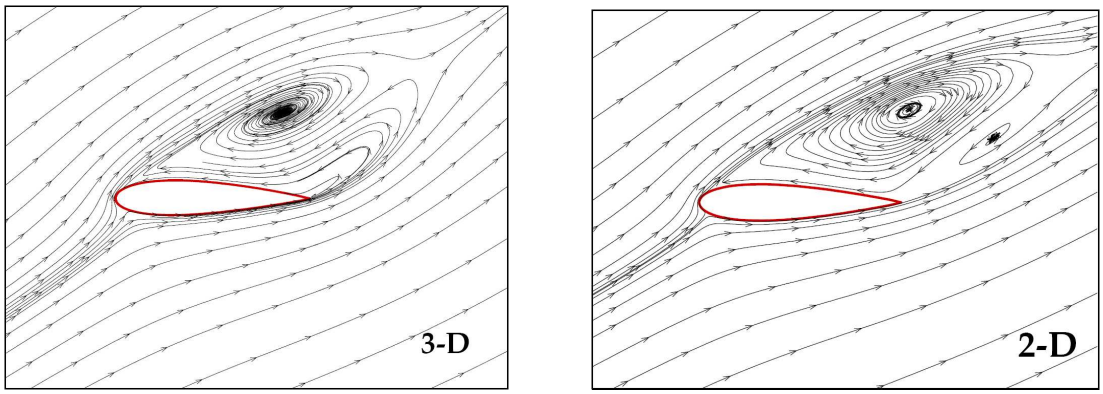

Figure 6. Streamlines around the 3–D rotating blade section at $r/R = 0.16$ and the corresponding 2–D case, with local incidence of 26.9 degrees and Reynolds number about 10^6.

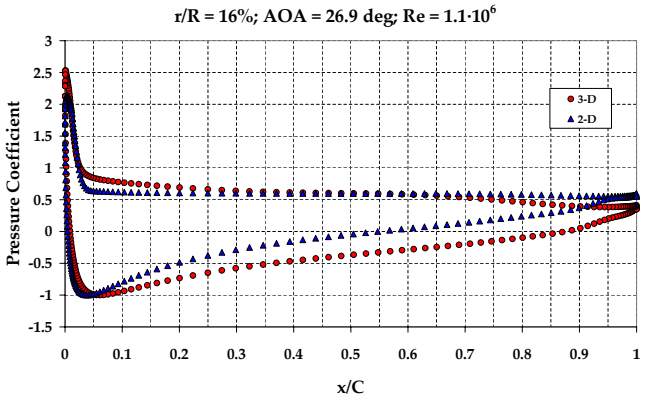

Figure 7. Pressure coefficient distribution of the 3–D rotating blade section at $r/R = 0.16$ compared to the 2–D case (angle of attack = 26.9 degrees, Reynolds number = 10^6).

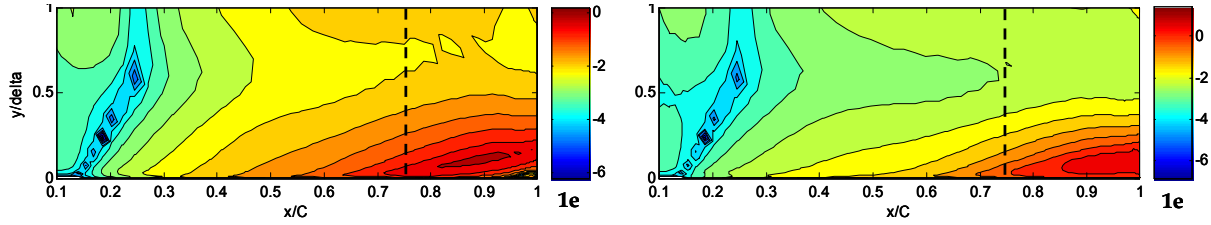

Figure 8. Relative magnitude of crossflow derivative (*left*) and Coriolis term (*right*) in the boundary layer momentum equations, in logarithmic scale. Separation is marked with a black dashed line.

explained because the 2–D section is isolated, while in the corresponding three-bladed rotor the local lift coefficient is increased due to a *cascade* effect. Moreover, in spite of the magnitude of the domain, boundary conditions could play an important role in influencing the flow field. In fact the wind turbine has been modeled as a sort of *ducted* machine, rather than an open–flow rotor like it is in the real case. As is concluded from Figure 9, this drawback could be overcome if we regard at a sufficiently outboard section (*e.g.* $r/R = 0.76$) as a reference 2–D situation.

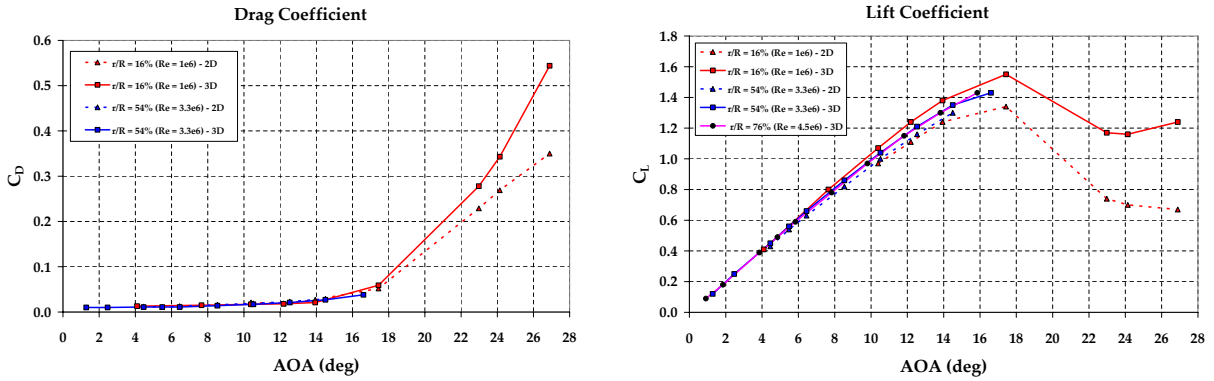

Figure 9. Drag and lift coefficients for the 3–D rotating blade sections at $r/R = 0.16$, 0.56 and 0.76 and the corresponding 2–D case. In the x-axis is the effective angle of attack.

4. Conclusions

The actual design approach for wind turbines is typically based on employing the blade–element momentum (BEM) theory, with lift and drag forces determined from 2–D measurements. Although CFD is not a practical design tool, useful suggestions for classical design codes can be derived, based on a quantitative explanation of rotational phenomena.

In this paper the full CFD–RANS approach has been followed to solve the flow field past the rotating blade of a wind turbine blade and for investigating the rotational effects in its the boundary layer. A useful postprocessing tool for studying the local velocity profiles and for evaluating quantitatively the terms of interest in the boundary layer equations has been implemented. For instance, the integral properties of boundary layer will be analyzed in order to find practical suggestions for design procedures. The early results for a simple blade geometry have been presented, confirming that 3–D loads on a rotating blade are higher than the corresponding non-rotating case, mostly for inboard sections and separated flow conditions. A more detailed analysis of the results is still in progress. Further flow situations (Reynolds number, angle of attack and rotational speed) will be studied for the actual geometry. The planned development includes the study of a more realistic model, *i.e.* a twisted and tapered rotating blade, based on the NACA 63–415 airfoil.

Acknowledgments

This project has been partially supported by DCAMM, the *Danish Center for Applied Mathematics and Mechanics.*

References

[1] Snel H, Houwink R, Bosschers J, Piers W J, van Bussel G J W and Bruining A 1993 Sectional prediction of 3-D effects for stalled flow on rotating blades and comparison with measurements *Proc. of EWEC* 395–9

[2] Harris F D 1966 Preliminary study of radial flow effects on rotor blades *J. of the American Helicopter Society* **11**(3) 1–21

[3] Himmelskamp H 1945 *Profile investigation on a rotating airscrew* (Göttingen: PhD Dissertation)

[4] Ronsten G 1992 Static pressure measurements on a rotating and non-rotating 2.375 m wind turbine blade. Comparison with 2D calculations *J. Wind Engineering and Industrial Aerodynamics* **39**(1-3) 105–18

[5] Tangler J L and Kocurek J D 2005 Wind turbine post-stall airfoil performance characteristics guidelines for Blade-Element Momentum methods *Proc. of 43rd AIAA Aerospace Sciences Meeting and Exhibit* (591) 1–10

[6] Sears W R 1950 Potential flow around a rotating cylindrical blade *J. Aeronautical Sciences* (Readers' Forum) **17**(10) 599

[7] Fogarty L E and Sears W R 1950 Potential flow around a rotating, advancing cylinder blade *J. Aeronautical Sciences* (Readers' Forum) **17**(10) 599
[8] Fogarty L E 1951 The laminar boundary layer on a rotating blade *J. Aeronautical Sciences* **17**(3) 183
[9] Banks W H H and Gadd G E 1963 Delaying effects of rotation on laminar separation *AIAA Journal* **1**(4) 941–2
[10] McCroskey W J and Dwyer H A 1969 *Methods of analyzing propeller and rotor boundary layers with crossflows* NASA SP-228 473–514
[11] Sørensen J N 1986 Prediction of the three-dimensional stall on wind turbine blade using three-level, viscous-inviscid interaction model *Proc. of EWEC* 429–35
[12] Shen W Z and Sørensen J N 1999 Quasi-3D Navier-Stokes model for a rotating airfoil *J. of Computational Physics* **150** 518–48
[13] Chaviaropoulos P K and Hansen M O L 2000 Three-dimensional and rotational effects on wind turbine blades by means of a Quasi-3D Navier-Stokes solver *J. of Fluid Engineering* **122** 330-6
[14] Du Z and Selig M S 2000 The effect of rotation on the boundary layer of a wind turbine blade *Renewable Energy* **20** 167–81
[15] Hu D, Hua O and Du Z 2006 A Study on stall-delay for horizontal axis wind turbine *Renewable Energy* **31** 821–36
[16] Lindenburg C 2004 Modelling of rotational augmentation based on engineering considerations and measurements *Proc. of EWEC*
[17] Bak C, Johansen J and Andersen P B 2006 Three-dimensional corrections of airfoil charcteristics based on pressure distributions *Proc. of EWEC*
[18] Schlichting H 1955 *Boundary layer theory* (New York: McGraw-Hill) 120–1
[19] Batchelor G K 1967 *An Introduction to Fluid Dynamics* (Cambridge University Press) 139–40
[20] Hansen M O L, Sørensen N N, Sørensen J N and Michelsen J A 1997 Extraction of lift, drag and angle of attack from computed 3-D viscous flow around a rotating blade *Proc. of EWEC* 499–502
[21] Johansen J and Sørensen N N 2004 Airfoil characteristics from 3D CFD rotor computations *Wind Energy* **7** 283–94
[22] Shen W Z, Hansen M O L and Sørensen J N 2006 Determination of Angle of Attack (AOA) for rotating blades *Proc. of Euromech Colloquium (Wind Energy)* 205–9
[23] Stock H W and Haase W 1999 Feasibility study of e^N transition prediction in Navier-Stokes methods for airfoils *AIAA Journal* **37**(10) 1187–96